Modelling Temperature Distribution in Multi-track Multi-layer Selective Laser Melted Parts: A Finite Element Approach

Anuj Kumar and Mukul Shukla

Abstract Selective laser melting (SLM) is an additive manufacturing (AM) process suited for printing three-dimensional metallic components. Throughout the SLM process, the thermal characteristics are crucial in ensuring the build quality of the print. Therefore, it becomes essential to determine the temperature distribution of the SLMed parts. Experimental approaches to address this issue are capital and time intensive. Numerical modelling studies for temperature distribution generally simulate single tracks, which cannot be extrapolated for the whole SLMed part. In this study, the multi-track, multi-layer SLM builds of IN718 were simulated using a three-dimensional finite element model. The temperature-dependent material properties were considered in modelling, and the laser scanning beam was described as a moving volumetric heat source. The temperature distribution on printed layers was evaluated, after which thermal profiles from simulated layers were extracted, and the permissible limit exercise was performed to identify potential hotspots. The predicted thermal history can also be used to optimise SLM process parameters. Further, the effects of scan strategy (layer start and rotation angle) on the temperature distribution were studied. It is evident from the results that the layer rotation angle affects the thermal history as the length of the scan vector changes depending upon the scan strategy used in a layer. This modelling approach can be utilised to further develop the microstructure evolution based on the simulated thermal history for SLMed parts.

Keywords Additive manufacturing · IN718 · Selective laser melting · Thermal history

A. Kumar · M. Shukla (✉)
Department of Mechanical Engineering, Motilal Nehru National Institute of Technology Allahabad, Prayagraj, India
e-mail: mukulshukla@mnnit.ac.in

M. Shukla
Department of Mechanical and Industrial Engineering Technology, University of Johannesburg, Johannesburg, South Africa

1 Introduction

Metal additive manufacturing also known as MAM demonstrated remarkable ability in the fabrication of metal objects with complex geometry [1]. The geometric versatility of MAM stems from the layer-by-layer scanning of a heat source, which generally melts the metal powder or wires [2]. Among the different MAM processes flourishing, selective laser melting (SLM) offers advantages in developing fully dense, near-net-shape metallic parts [3]. The high-energy laser scans the previously placed powder layer, melting the powder particles beneath the beam, which leads to the creation of a melt pool [4]. A fine track of solid metal is developed as the laser beam travels, and by repeating these scans, the entire part is fabricated [5].

Nickel-based superalloys have become more prevalent in pivotal industries like aerospace, marine, and nuclear [6]. Due to its potential to retain its high strength at elevated temperatures, Inconel 718 (IN718) has gained acceptance in many applications [7]. SLM fabrication of IN718 components has addressed many of the challenges associated with conventional manufacturing methods [8]. However, the challenge regarding the process-induced defects, microstructure, and property relationships with process parameters and dimensional accuracy is still there for SLMed parts [9].

One viable approach for limiting or eliminating SLM defects and achieving higher build quality is to determine the temperature of melt pool during printing and control it accordingly. Further, the resulting microstructure and properties of SLMed parts are strongly influenced by temperature distribution, as it governs the solidification characteristics and grain growth [10]. The thermal history is also shown to have a strong effect on melt pool geometry and hence the dimensional accuracy of the SLMed parts [11]. Temperature distribution is also used in residual stress evaluation, grain growth estimation, and process parameter optimisation, in addition to assessing and limiting defects [12]. Thus, it is evident that temperature distribution plays an important role in realising defect free SLM builds, and therefore, an efficient framework is desired that can predict temperature distribution with a given set of process parameter condition. Several researchers incorporated different frameworks to obtain temperature profiles using experimental, analytical, and numerical approaches [13].

In the experimental domain, researchers started to monitor thermal history with the help of various sensors to observe in situ control of build quality [14]. Incorporating various monitoring sensors into the SLM setup and analysing the generated data is both costly and time intensive [15]. Therefore, developing rapid and cost-effective numerical modelling approaches to predict temperature distribution is so critical in the context of SLM.

Various multiscale modelling frameworks are also developed to study the temperature distribution in SLM builds [16]. These numerical models seem to be reliable to predict the thermal history in SLM because they also reveal the underlying physics of the process [17]. Studies using numerical modelling techniques for various combinations of process parameters on various material systems are documented in the literature [18, 19]. A numerical model with a Gaussian heat source is developed for a
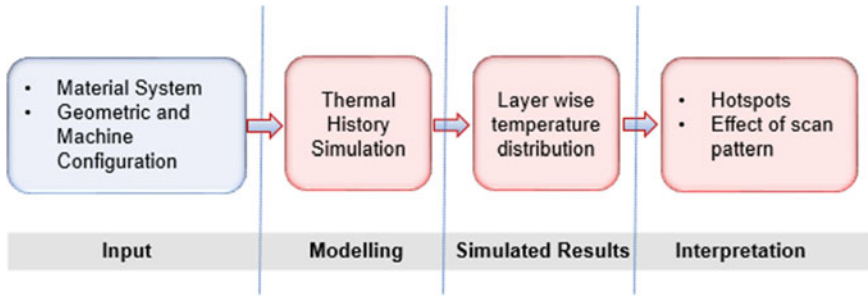
Fig. 1 Modelling framework used in the study

single bead print to predict the effect of important process conditions on SLM build [20]. In another study, a thermal simulation model is employed to assess the influence of scan speed on the developed solidification characteristics in the SLM parts [21]. The thermal model is useful to predict the temperature distribution as well as to develop the linkage between process parameters and the developed thermal history [22]. Zhao [23] used a FEM-based numerical model to foresee the residual stresses based on the thermal history during the printing of titanium alloy. Tan [24] proposed a thermo-microstructural model to determine the temperature history and grain growth for various SLM process parameters.

It is evident from the literature that several studies have been conducted on predicting the thermal history as a signature for various outcomes, including grain growth, distortion, residual stress, and quality control. But the point-wise temperature distribution or nodal thermal history is not yet fully explored by numerical modelling, and hence there is a need for an efficient approach to model temperature distribution in SLM builds. In this study, the multi-track, multi-layer SLM builds of IN718 were simulated using a three-dimensional FEM model. The temperature distribution on printed layers was evaluated, after which thermal profiles from simulated layers were extracted and the permissible limit exercise was performed to identify potential hotspots. Additionally, the impact of the layer rotation angle or scan pattern on the simulated thermal history was investigated. Figure 1 depicts the framework employed in the study.

2　Material and Methods

For thermal analysis, some physical assumptions related to the SLM process were taken into account. The physical characteristics of the powder particles were homogeneous, and the powder bed was regarded as a continuous media. The numerical modelling takes into account the material's temperature-dependent thermophysical properties. The convective heat transfer coefficient for the powder bed was assumed

to be constant. The material data for IN718 with thermophysical properties was taken from the ANSYS mechanical engineering data source.

2.1 Governing Equations

Various key SLM process parameters such as laser power (P), scanning speed (v), hatch spacing (h), and layer thickness (t) are related to laser energy density (E_d) as:

$$E_d = \frac{P}{v.t.h} \text{J/mm}^3 \tag{1}$$

The partial differential equation for the transient heat transfer satisfied by the temporal and spatial distribution of the temperature field is given by [25]:

$$\rho c \frac{\partial T}{\partial t} = \frac{\partial}{\partial x}\left(k\frac{\partial T}{\partial x}\right) + \frac{\partial}{\partial y}\left(k\frac{\partial T}{\partial y}\right) + \frac{\partial}{\partial z}\left(k\frac{\partial T}{\partial z}\right) + Q \tag{2}$$

where T is the temperature, t is the interaction time, and ρ, c, k are material density, heat capacity, and thermal conductivity, respectively. Q represents the volumetric heat generation.

The initial state of the temperature distribution can be written as-

$$T(x, y, z, t)_{t=o} = T_0 \tag{3}$$

where T_0 is the ambient temperature. The following is a representation of the natural boundary condition with energy balance:

$$k\frac{\partial T}{\partial z} + h(T - T_0) + \sigma\varepsilon(T^4 - T_0^4) = Q \tag{4}$$

where h is the coefficient of convective heat transfer, ε is the emissivity of the surface, and σ represent the Stefan–Boltzmann constant.

It was assumed that the surface heat flux distribution throughout the powder bed follows a Gaussian distribution and is expressed by [26]

$$Q_0 = \frac{32AP}{\pi D^2} \exp\left(\Delta\frac{2r^2}{D^2}\right) \tag{5}$$

where $A, P,$ and D represent the energy absorption coefficient, laser power, effective laser spot diameter. Further, r represents the radial distance between a point on the powder bed and laser spot.

2.2 Thermal History Simulation

The thermal history in the SLM builds was simulated by generating elemental temperature distributions on individual layers of the build. In this approach, results from a coaxial average sensor were simulated, comprising the temperature distribution for an arbitrary layer within the build with a given material system and process parameter combination. A simulated map of the instantaneous temperatures was generated within a circular field of view centred around the laser at the top surface of the build. Temperatures were averaged over the field of view radius, which was defined by the sensor radius, an input parameter. The average temperature will generally decrease as the sensor radius is increased since the thermal gradients are strongest in the melt pool vicinity.

First, a 3 mm cube was designed using 3D CAD modelling software, Ansys SpaceClaim, and imported into the numerical simulation module. The designed cube and considered layer for temperature distribution are shown in Fig. 2. Then a thermal model was employed with all the input process parameters given in Table 1. Sensor radius of 0.2 mm and the layer at 2 mm height from the bottom was considered for temperature distribution modelling.

To further study the influence of the scan pattern or layer rotation angle, three adjacent layers, starting from the bottom layer, were simulated. As the layer start angle and layer rotation angle are 57° and 67°, the first three layers have starting angles of 57°, 124°, and 181°, respectively. The centre point on the individual layer
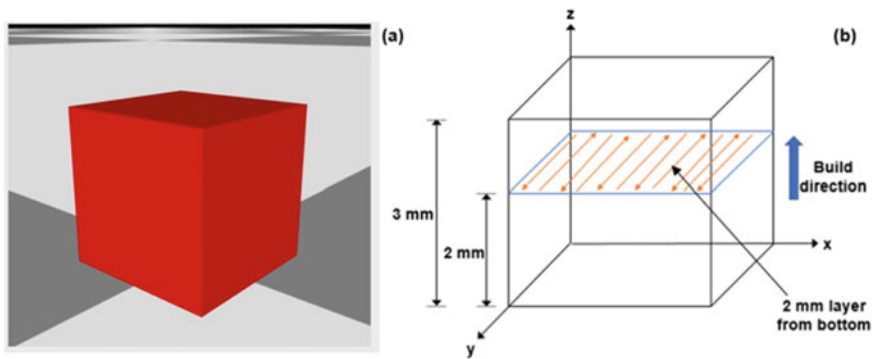
Fig. 2 Representation of **a** 3 mm cube and **b** the layer at 2 mm from the bottom considered for the temperature distribution

Table 1 Process parameters used for thermal simulation

Laser power (W)	Scan speed (mm/s)	Layer thickness (μm)	Hatch spacing (μm)	Base plate temperature (°C)	Laser spot size (μm)	Layer start/ rotation angle (°)
200	900	30	120	80	100	57/67
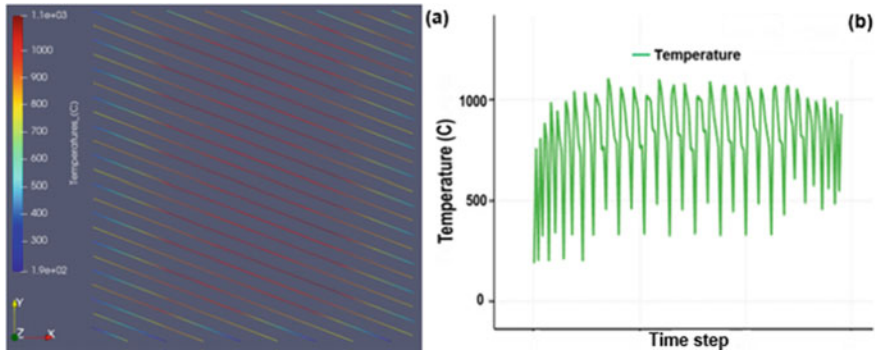
Fig. 3 Representation of **a** thermal history and **b** variation of temperature with time during print

was considered for the comparison, and the temperature at that point is taken as T_{point}. Moreover, the maximum temperature on each individual layer (T_{max}) was also used to compare the thermal history of these layers. The individual layer results and comparative study are discussed in the next section.

3 Results and Discussions

3.1 Thermal History

By analysing the output visualisation toolkit files, the temperature distribution on the printed layer was predicted. The temperature distribution outputs for a layer at 2 mm from the bottom are shown in Fig. 3. Figure 3a depicts the temperature distribution over the whole layer, whereas Fig. 3b shows the fluctuations in the temperature as the layer is printed.

Further, domains from the individual layer were extracted, and the permissible limit exercise was performed to find out the potential hotspots. The extracted domain from the layer at 2.0 mm height from the base is shown in Fig. 4, along with spots where the local temperature surpasses 1050 °C.

3.2 Effect of the Scan Pattern on the Thermal History

Individual layer results from three adjacent layers starting from the bottom layer are shown in Table 2. The temperature at the centre point of the layers (T_{point}) is increasing as the next layer is printed. T_{point} for the first layer is 988.5 °C, whereas for second layer it is significantly increased to 1049.3 °C (Figs. 5 and 6). This is due to the additional heating provided by the previously deposited layer. Similarly,
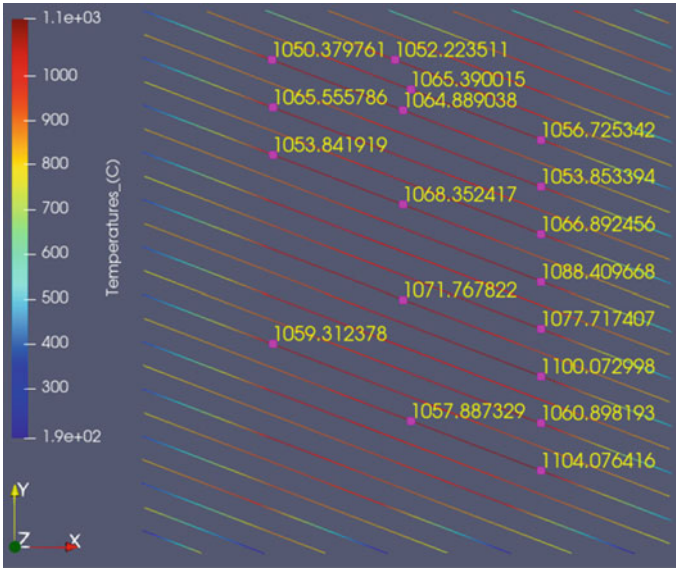
Fig. 4 2 mm layer from the bottom showing hotspots where local temperature exceeds 1050 °C

Table 2 Effect of scan pattern on thermal history

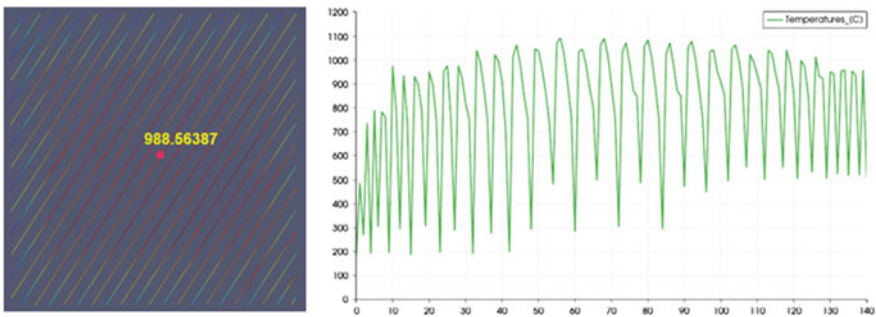| Layer	Layer start angle (°)	T_{point} (°C)	T_{max} (°C)
1	57	988.5	1066.1
2	124	1049.3	1119.5
3	191	1077.8	1127.3

Fig. 5 Temperature distribution on the first layer from base with T_{point}

the temperature of the third layer is increased to 1077.8 °C (Fig. 7). The thermal impact of the residual heat from deposited layers can also be seen in the maximum temperature (T_{max}), which is also increasing as second and third layers are printed.
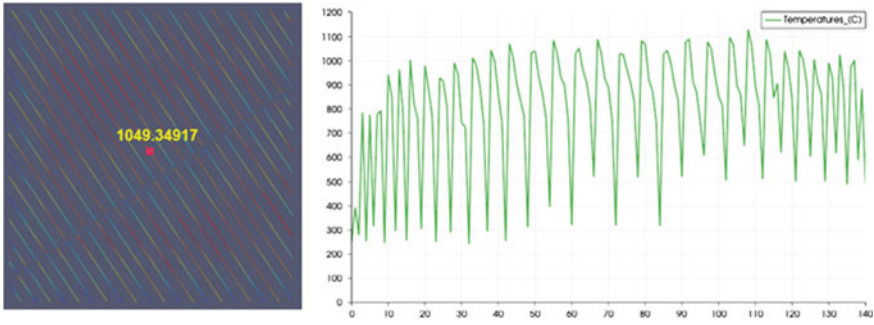
Fig. 6 Temperature distribution on the second layer from with T_{point}
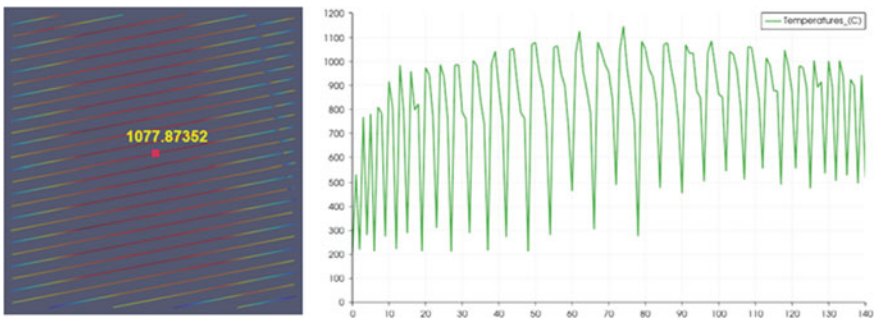
Fig. 7 Temperature distribution on the third layer from base with T_{point}

The individual layer scans show how the layer rotation angle alters the number of tracks on a layer and also the length of an individual track. It demonstrates that any arbitrary point on the layer experiences a significantly different temperature history depending on the layer start and rotation angles. The effects of this altered temperature distribution can be seen in the developed residual stresses and distortion, but these outcomes are not in the scope of current study.

4   Conclusion

In this work, a numerical modelling approach was employed to study the temperature distribution in multi-track, multi-layer SLMed IN718. The simulated thermal history, corresponding to SLM process parameters, was further utilised in conducting permissible limit exercise and potential hotspots identification. These hotspots where the local temperature exceeds the permissible limit can be attributed to the potential process-induced defects commonly found in SLMed parts. Hence, this thermal history simulation can be utilised prior to the actual printing of SLMed parts to assess

the temperature distribution and hotspots and optimise the SLM input parameters accordingly. Further, the effect of the scan pattern was also analysed by considering the temperature at the centre point and the maximum temperatures of individual adjacent layers. The different thermal histories in these layers are attributed to residual heat from previous layers and a change in the length of scan vectors due to different layer start and rotation angles.

References

1. Bandyopadhyay A, Heer B (2018) Additive manufacturing of multi-material structures. Mater Sci Eng R Rep 129(17):1–16
2. Yusuf SM, Cutler S, Gao N (2019) The impact of metal additive manufacturing on the aerospace industry. Metals 9:1286
3. Sefene EM (2022) State-of-the-art of selective laser melting process: a comprehensive review. J Manuf Syst 63:250–274
4. Kumar S, Maity SR, Patnaik L (2021) Mechanical and scratch behaviour of TiAlN coated and 3D printed H13 tool steel. Adv Mater Proc Technol 8(2):337–351
5. Frazier WE (2014) Metal additive manufacturing: a review. J Mater Eng Perform 23:1917–1928
6. Teixeira O, Silva FJG, Atzeni E (2021) Residual stresses and heat treatments of Inconel 718 parts manufactured via metal laser beam powder bed fusion: an overview. Int J Adv Manuf Technol 113:3139–3162
7. Lambarri J, Leunda J, Garcia-Navas V, Soriano C, Sanz C (2013) Microstructural and tensile characterization of Inconel 718 laser coatings for aeronautic components. Opt Lasers Eng 51(7):813–821
8. Wang X, Gong X, Chou K (2017) Review on powder-bed laser additive manufacturing of Inconel 718 parts. Proc Inst Mech Eng Part B: J Eng Manuf 231(11):1890–1903
9. Jaber H, Kovacs T, Janos K (2022) Investigating the impact of a selective laser melting process on Ti6Al4V alloy hybrid powders with spherical and irregular shapes. Adv Mater Proc Technol 8(1):715–731
10. Gao S, Yan X, Chang C, Aubry E, Liu M, Liao H, Fenineche N (2021) Effect of laser energy density on surface morphology, microstructure, and magnetic properties of selective laser melted Fe-3wt.% Si Alloys. J Mater Eng Perform 30(7):5020–5030
11. Dilip JJS, Zhang S, Teng C, Zeng K, Robinson C, Pal D, Stucker B (2017) Influence of processing parameters on the evolution of melt pool, porosity, and microstructures in Ti-6Al-4V alloy parts fabricated by selective laser melting. Prog Additive Manuf 2:157–167
12. Zhang X, Mao B, Mushongera L, Kundin J, Liao Y (2021) Laser powder bed fusion of titanium aluminides: an investigation on site-specific microstructure evolution mechanism. Mater Des 201:109501
13. Spears TG, Gold SA (2016) In-process sensing in selective laser melting (SLM) additive manufacturing. Integrating Mater Manuf Innovat 5:16–40
14. Shrestha S, Chou K (2018) Single track scanning experiment in laser powder bed fusion process. Proced Manuf 26:857–864
15. Scime L, Beuth JL (2019) Melt pool geometry and morphology variability for the Inconel 718 alloy in a laser powder bed fusion additive manufacturing process. Addit Manuf 29:100830
16. Khairallah SA, Anderson AT (2014) Mesoscopic simulation model of selective laser melting of stainless-steel powder. J Mater Process Technol 214:2627–2636
17. Khairallah SA, Anderson AT, Rubenchik A, King WE (2016) Laser powder-bed fusion additive manufacturing: physics of complex melt flow and formation mechanisms of pores, spatter, and denudation zones. Acta Mater 108:36–45

18. Wang N, Shen J, Hu S, Liang Y (2020) Numerical analysis of the TIG arc preheating effect in CMT based cladding of Inconel 625. Eng Res Express 2(1):015030

19. Jelvani S, Razavi RS, Barekat M, Dehnavi M (2020) Empirical-statistical modelling and prediction of geometric characteristics for laser-aided direct metal deposition of Inconel 718 superalloy. Met Mater Int 26(5):668–681

20. Patil RB, Yadava V (2007) Finite element analysis of temperature distribution in single metallic powder layer during metal laser sintering. Int J Mach Tools Manuf 47(7):1069–1080

21. Gusarov AV, Yadroitsev I, Bertrand P, Smurov I (2007) Heat transfer modelling and stability analysis of selective laser melting. Appl Surf Sci 254(4):975–979

22. Arisoy YM, Criales LE, Ozel T (2019) Modelling and simulation of thermal field and solidification in laser powder bed fusion of nickel alloy IN625. Opt Laser Technol 109:278–292

23. Zhao X, Iyer A, Promoppatum P, Yao SC (2017) Numerical modelling of the thermal behaviour and residual stress in the direct metal laser sintering process of titanium alloy products. Addit Manuf 14:126–136

24. Tan P, Shen F, Li B, Zhou K (2019) A thermo-metallurgical-mechanical model for selective laser melting of Ti6Al4V. Mater Des 168:107642

25. Li Y, Gu D (2014) Parametric analysis of thermal behaviour during selective laser melting additive manufacturing of aluminium alloy powder. Mater Des 63:856–867

26. Yin J, Zhu H, Ke L, Lei W, Dai C, Zuo D (2012) Simulation of temperature distribution in single metallic powder layer for laser micro-sintering. Comput Mater Sci 53(1):333–339